Genetically Encoded Hydrogels with Tunable Viscoelasticity and Biodegradability for Injectable Cell Therapies

Jennifer Irvin Bennett

A thesis

submitted in partial fulfillment of the

requirements for the degree of

Master of Science in Chemical Engineering

University of Washington

2021

Reading Committee:

Cole A. DeForest, Chair

Elizabeth Nance

Program Authorized to Offer Degree:

Chemical Engineering

University of Washington

Abstract

Genetically Encoded Hydrogels with Tunable Viscoelasticity and Biodegradability for Injectable Cell Therapies

Jennifer Irvin Bennett

Chair of the Supervisory Committee:
Weyerhaeuser Endowed Associate Professor, Cole A. DeForest
Chemical Engineering and Bioengineering

The widespread prevalence of heart disease, as well as the heart's inability to regenerate, continues to present a global burden on human health. Therapeutic strategies involving direct injection of stem cell-derived cardiomyocytes into damaged heart muscle significantly outperform acellular strategies in restoring cardiac function post myocardial infarction. Although such cell-based therapies exhibit great promise, long-term survival and engraftment of the injected cardiomyocytes in state-of-the-art formulations remains low (~10%). Towards improving general efficacy of cell therapies, this thesis introduces a self-healing genetically encoded protein-based hydrogel biomaterial that supports minimally invasive cell delivery through catheter injection and enhanced biological function. Exploiting non-covalent self-association of monomeric recombinant proteins to yield stable hydrogels, the simple design is modular and tunable, whereby single point mutations to protein primary sequence produce materials with significantly varied self-healing

behavior and biodegradability. Furthermore, the hydrogel can be readily functionalized with bioactive proteins of interest to facilitate specific cell fates and enhanced engraftment. Overall, these materials offer exciting opportunities towards promoting patient recovery after heart attack.

TABLE OF CONTENTS

LIST OF FIGURES

LIST OF TABLES

ACKNOWLEDGEMENTS

First and foremost, I would like to express my deepest appreciation to my supervisor Dr. Cole DeForest for all of his guidance throughout my studies. His knowledge in the field of biomaterials and protein engineering paired with his upbeat encouragement has been invaluable in my thesis work. I would also like to extend my sincere thanks to Dr. Elizabeth Nance for serving on my committee and for her insightful comments and suggestions on this thesis. I am deeply grateful for Mary Boit's mentorship in graduate school and for her instrumental contributions by training me on various lab techniques and consulting with me on a frequent basis. I am also grateful to my lab mates, current and past, for their practical and insightful suggestions – particularly Ross Bretherton and Nicole Gregorio. Finally, I would like to thank my husband, my parents, and my siblings. Without their support and encouragement, this thesis would not be possible.

DEDICATION

I dedicate this thesis to my mom, for her endless support to me during undergraduate and graduate studies.

Chapter 1. INTRODUCTION

Heart failure remains the number one killer in the world and accounts for 9.4 million deaths annually, including 650,000 in the United States[1,2]. This disease usually manifests during a heart attack, clinically known as a myocardial infarction (MI). During an MI, the human heart loses one billion cardiomyocytes on average which are replaced by maladaptive fibrotic scar tissue, resulting in loss of pumping power and capacity[3]. Current treatment options are palliative at best: revascularization by catheters, palliative drug regimens (e.g., ACE Inhibitors, Beta Blockers), or ventricular assist devices[4]. Organ transplant remains the only true cure currently available which is significantly limited by donor supply[3]. In addition, organ transplant is extremely invasive and requires harsh drug regimens of immunosuppressants to lower the risk of organ rejection. Therefore, there is an outstanding need for a more innovative treatment option.

Injectable cell-therapies are an appealing and exciting new category of treatments in development for heart disease, as well as a variety of other illnesses. In the past, injection of noncardiomyocyte cell types to an ischemic heart showed initial positive effects, however, it did not indicate improvement long term[4]. On the other hand, cell-based therapies involving cardiac-derived cells, such as cardiac stem cells (including progenitor cells) and cardiospheres, have shown functional improvement in the pumping capacity of the heart, though their long-term retention remains low[4]. Most promising thus far have been induced pluripotent stem cell-derived cardiomyocytes (iPSC-CMs), which have demonstrated long-term survival and have been shown to electrically couple with the host, unlike prior therapies[3–5].

The Murry group has developed an injectable system of iPSC-CMs as a single-cell liquid suspension (10 million cells/rat; 1 billion/pig; 1 billion/macaque monkey) within a pro-survival cocktail consisting of essential factors for cell survival (anti-apoptotic peptide Bcl-XL,

immunosuppressant cyclosporine A, ischemic preconditioning molecule pinacidil, and caspase inhibitor ZVAD-fmk)[5]. These injections resulted in 10% retention of implanted cells three months post-transplantation, which ultimately resulted in an 11% increase in cardiac function measured via ejection fraction, or the amount of blood pumped with each beat[5,6]. This improvement in cardiac function is better than any other therapy on the market to date; 6% improvement alone will take a bed-ridden patient back to a quality of life such that they can independently perform daily actions without a caretaker.

However, despite this progress, there are still outstanding limitations of injectable iPSC-CM therapies including the need to improve cell survival and retention above 10%. Particularly, the current delivery method of cells within a liquid does not protect the cells during injection, nor does it stabilize them once implanted within a 3D space. This leads to poor engraftment and high manufacturing costs due to loss of cells. Cell survival and retention could be significantly improved with the use of an injectable biomaterial platform. Injectable materials are quite appealing due to their ability to be delivered through a catheter, provide cell protection from mechanical forces of shear through the needle, and also supply a scaffold for the cells to stabilize once injected[7].

Many injectable biomaterial candidates have been explored to improve the efficiency of cell therapies. One such approach achieved a three-fold increase in graft size by encapsulating iPSC-CMs within collagen-based hydrogels during injection[8]. While promising, natural protein-based hydrogels including collagen lack many of the desirable material properties (e.g., stiffness, handleability) and controllable parameters (e.g., biodegradation rate)[9,10]. Additionally, natural protein-based biomaterials present batch-to-batch variability issues for manufacturing purposes.

This is where the use of synthetic and genetically encoded materials come into play, which may further enhance cell engraftment and reduce the number of cells required for implantation.

1.1 INJECTABLE BIOMATERIALS

Injectable biomaterials can be comprised of natural and synthetic materials that are either physically or chemically crosslinked[11,12]. Naturally derived injectable materials include collagen, gelatin, alginate, Matrigel, and fibrin[8,13]. Synthetic injectable materials include poly(ethylene glycol) (PEG), zwitterionic polymers (e.g., polycarboxybetaine, sulfobetaine, 2-methacryloyloxyethyl phosphorylcholine), poly(2-hydroxyethyl methacrylate) (PHEMA), poly(N-isopropylacrylamide) (PNIPAAM), chemically modified hyaluronic acid (HA), synthetically modified gelatin, and recombinant proteins[14–19]. The material's mode of injectability can be thermo-responsive, pH-responsive, physically responsive (shear-thinning and self-healing), or a combination of all three properties[20]. Injectable hydrogels have enhanced cell therapies as demonstrated by polysaccharide-based gels for neural stem cells, zwitterionic-based gels for hematopoietic stem cell transplantation for leukemia patients, and reversible PEG gels for differentiation of mesenchymal stem cells[16,21,22].

Materials historically used in cardiac treatment consist of (a) acellular gels, (b) acellular gels with a biological attachment molecule, (c) gels encapsulating non-cardiomyocyte cell-type therapies, and (d) gels encapsulating cardiomyocyte cell-therapies. (a) Examples of acellular gel materials include sterically constrained cyclic peptides and VentriGel[23,24]. While these materials have been shown to reduce infarct size, they are limited to only slowing down the death of native tissue as a physical barrier. (b) Other materials have been combined with biological cardiac specific factors such as collagen gels functionalized with Delta-1/Notch-1 (involved in cell-cell signals with regeneration pathways after injury) and PEG gels functionalized with erythropoietin

(EPO) (a hormone to stimulate red blood cell production)[8,25]. These materials have further enhanced cellular function in the native heart by providing relevant biological cues to native cells needed to prevent further damage. (d) Other materials have utilized combinations of these gels with non-cardiomyocyte cell-therapies such as modified hyaluronic acid (HA) with endothelial progenitor cells (EPCs) to promote vascularization or cardiospheres within HA to promote cardiac cell survival and regeneration cues[15,26]. While these cell types provide other utilities to the heart, they do not solve the underlying problem of improving overall pumping power. (d) Thus, using a combination of these approaches of hydrogels and encapsulating the most relevant cells, iPSC-CMs, has greatest potential for long-term engraftment and ultimately improve the pumping capacity of the heart.

1.2 COILED-COIL XTEN BASED HYDROGEL

An ideal biomaterial for cell-therapies should be non-immunogenetic, biodegradable, and injectable, display tissue-like elasticity, and support living cells. The design of our system is a synthetic protein biomaterial consisting of a flexible linker flanked by coil domains, similar to the designs from Dr. David Tirrell and Dr. Peter Rapp[27–31]. The coil domains in our platform are derived from the N-terminal fragment of rat cartilage oligomeric matrix protein (COMP) and our flexible linker is XTEN, an unstructured protein evolved to mimic PEG (**Figure 1a**). We hypothesized that cell function could be improved through increased cell-material interactions, so we turned to RGD, a common peptide sequence responsible for cell adhesion found in fibronectin and other ECM proteins. The final construct was designed to include this RGD motif on both sides of the P domains to improve cell adhesion.

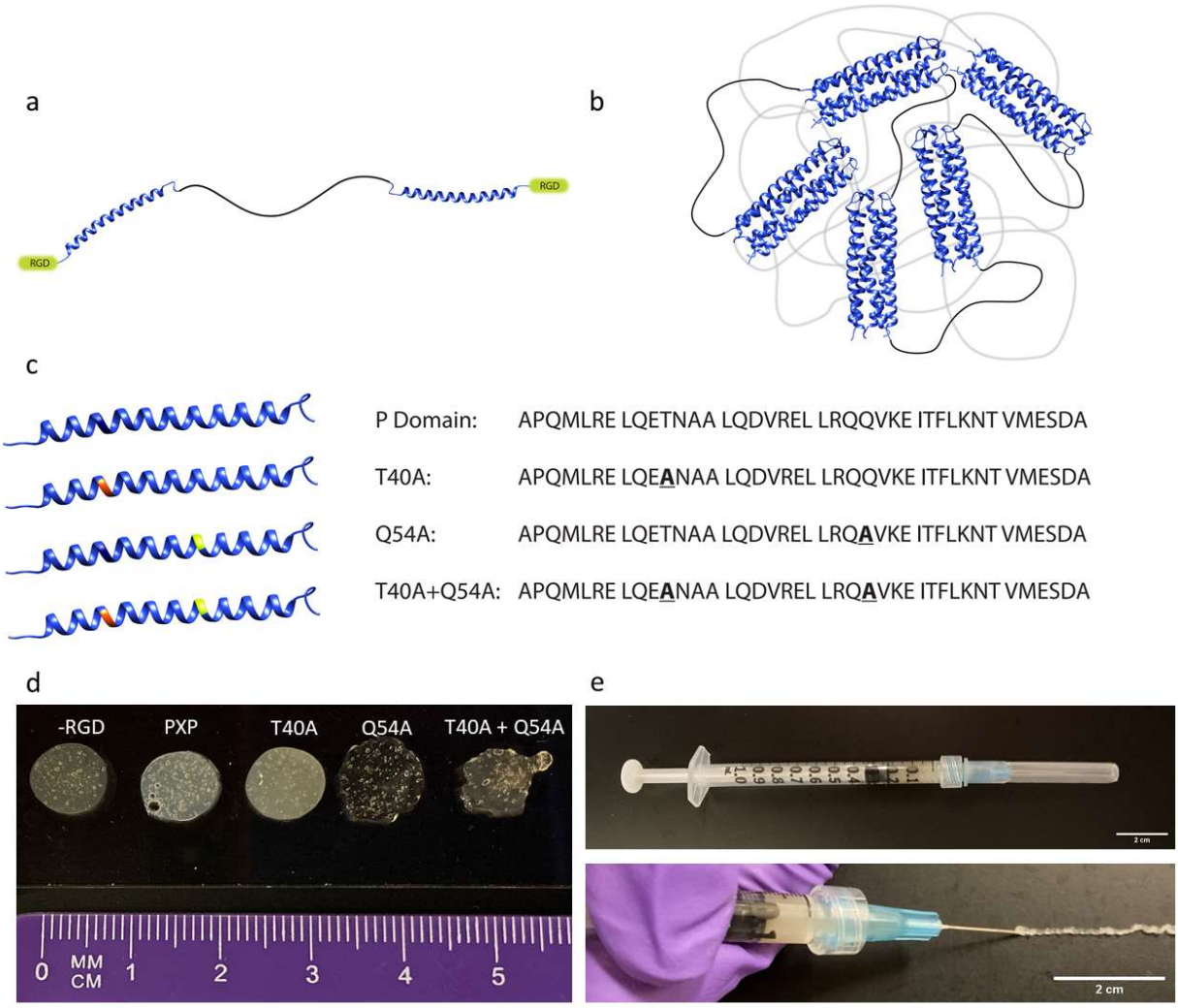

Figure 1. Coil-flexible linker-coil material design. a) RGD cell adhesion sites in green, P domains in blue, and XTEN in black. Monomer units self-associate to form a gel via b) homopentameric coiled-coil interactions (PDB 1VDF[32]). The PXP pentamers create a gel network, where the physical bonds can be broken under high shear stress and reformed upon return to low shear stress. c) Amino acid sequences of the original P domain and single point mutations (T40A in orange, Q54A in green, T40A + Q54A) for stabilizing the coiled-coil interactions. d) Images of PXP gels ± RGD and with mutations to enhance physical association between P domains. e) PXP gels are injectable through a 26 G needle.

The flexible linker, XTEN[33], is an engineered protein originally designed to extend the half-life of small molecule drugs as an alternative to PEG[34,35]. While PEG is commonly attached

to therapeutic proteins to increase half-life, it presents complications of heterogeneity in manufacturing, has shown to cause renal tubular vacuolation, and there is growing evidence of the presence of anti-PEG antibodies found from its overuse[36–38]. Consequently, researchers have explored alternative options, such as XTEN, as a genetically encoded strategy resulting in consistent manufacturing and lowered immune response (no detectable antibody response)[39]. XTEN is comprised of 36 residue pseudo repeats containing amino acids A, E, G, P, S, and T. The full length of XTEN is 864 amino acids, and protein conjugate circulation half-life can be adjusted by removing or adding pseudo repeats. XTEN's sequence was designed without hydrophobic amino acids (F, I, L, M, V, W, and Y), yielding a high-expressing nonimmunogenic protein with a flexible structure. Other amino acids were excluded to improve long-term stability (N, Q) and to avoid chains that bind to cell membranes (H, K, R)[33].

The coil P domains utilized here form homopentameric coiled-coil physical bonds[40,41]. By creating triblock ABA-type protein copolymers end-flanked with the P domain, injectable gels can be formed, and physically stabilized through the reversible association of the P units[27,42] (**Figure 1b**). The strength of these physical associations in the P domain can be modulated by single amino acid mutations within the coil sequence[28,43,44] (**Figure 1c)**. Mutation of two polar residues to a smaller hydrophobic Alanine were further explored to stabilize the helical structure by reducing steric interference between side chains[28,44]. We mutated the Threonine (T) residue in position 40 of COMP to Alanine (A) within each of the P domains in PXP, yielding a mutant protein denoted T40A. Similarly, mutation of the Glutamine (Q) residue in position 54 of COMP to Alanine (A) within each of the P domains, yielded a mutant protein designated as Q54A. Finally, mutation of both T in position 40 and Q in position 54 of COMP to A within each of the P domains yielded a protein mutant denoted T40A + Q54A. The P domains in our design (without T40A and Q54A

mutations) perfectly match the sequence of COMP in many species, including mouse, human, and rat, with the exception of two cysteine residues that have been mutated to serine to prevent disulfide bond formation and chemical cross-linking[29].

Chapter 2. MATERIALS AND METHODS

2.1 PLASMID CONSTRUCTION

The original plasmid encoding for $PX_{144}P$ (-RGD) (a truncated version of XTEN with only 144 residues, flanked by matching P domains and 6xHis tags) was gifted by Dr. Peter Rapp in a pQE-30 backbone (T5 promoter, ampicillin and chloramphenicol acetyltransferase resistance). Cell adhesion sites (GRGDS) were cloned into regions between the P domains and 6xHis tags on both ends resulting in $PX_{144}P$. Insertion at the N terminus was implemented through annealed oligo cloning with BamHI/SalI restriction sites (oligos from Integrated DNA Technologies/IDT). At the C terminus, Gibson Assembly of a GRGDS Gblock with overhangs was inserted at the BamHI/SalI restriction sites (Gblock from IDT).

For the introduction of point mutations in P domains, plasmids encoding for P domains in a pTwist Amp High Copy cloning vector (ampicillin resistance) were purchased from Twist Biosciences and a plasmid encoding for X_{144} was gifted by Dr. Peter Rapp in a pQE-30 backbone. Point mutations (T40A, Q54A, or both T40A + Q54A) were introduced by site-directed mutagenesis on P domain plasmids (primers from IDT). Mutated P domains were digested and inserted into the X_{144} plasmid at N terminal restriction sites BamHI/SalI and C terminal restriction sites XhoI/HindIII.

To model biofunctionalization, the plasmid encoding for PeGFP (enhanced green fluorescent protein with a single P domain and 6xHis tag) was purchased from GenScript in a pET-

21b(+) backbone (T7 promoter, ampicillin resistance). Deletion of the P domain in the PeGFP plasmid was executed via Gibson assembly to form eGFP with a 6xHis tag as a control that would not integrate with the pentameric bundles of the hydrogel network (primers from IDT). All cloning was confirmed by Sanger Sequencing (Genewiz, Inc.) and amino acid sequences can be found in **Table S1**.

2.2 PROTEIN EXPRESSION AND PURIFICATION

Plasmids were transformed into BL21(DE3) *E. coli* cells and protein was expressed in autoinducing media [42.3 mM Na_2HPO_4, 22.04 mM KH_2PO_4, 0.28 M tryptone, 18.23 mM yeast extract, 85.56 mM NaCl, 2.78 mM glucose, 5.84 mM lactose, 0.6% (v/v) glycerol, pH 7.2] supplemented with 0.1 mg mL^{-1} carbenicillin at 37 °C for 6 – 8 hours followed by 18 °C for 14 – 16 hours. Cell cultures were centrifuged and cell pellets were stored at -80 °C until purification.

Cell pellets were resuspended in equilibration buffer and lysed by sonication on ice (30% amplitude and 33% duty cycle). Clarified lysate was then purified by Ni-NTA affinity chromatography at room temperature. To remove endotoxins, the column was washed 5x with 5 column volumes (CV) of 0.1% Triton X-114 in equilibration buffer followed by 5x with 5 CV of equilibration buffer. Finally, the protein was eluted 4x with 2 CV of elution buffer.

$PX_{144}P$ and mutants (T40A, Q54A, and T40A + Q54A) were purified under standard conditions (equilibration buffer: 20 mM Tris, 50 mM NaCl, 10 mM imidazole, pH 8.0; elution buffer: 20 mM Tris, 50 mM NaCl, 250 mM imidazole, pH 8.0). The purified protein was dialyzed against deionized water, sterile filtered, flash frozen with liquid nitrogen, and lyophilized to yield a white solid corresponding to the final product.

PeGFP and eGFP proteins were purified under denaturing conditions adapted from a previous method (equilibration buffer: 0.1 M NaH_2PO_4, 10 mM Tris, 8 M urea, 10 mM imidazole,

pH 8.0; elution buffer: 0.1 M NaH_2PO_4, 10 mM Tris, 8 M urea, 250 mM imidazole, pH 4.44).[44] Purified proteins were refolded by a step-down in urea concentration during dialysis. Initially, the protein was dialyzed against 6 M urea in phosphate buffer (13 mM NaH_2PO_4, 86 mM Na_2HPO_4, pH 8.0), followed by 4 M urea in phosphate buffer, then 2 M urea in phosphate buffer, and finally against phosphate buffer without urea. The purified protein solution without urea was flash frozen with liquid nitrogen and stored at -80 °C.

2.3 PROTEIN VERIFICATION

Protein purity was assessed using sodium dodecyl sulphate–polyacrylamide gel electrophoresis (SDS-PAGE). Samples were diluted with 2X Laemmli sample buffer containing 2-mercaptoethanol as a reducing agent and boiled at 100 °C for 10 minutes prior to loading on the gel. SDS-PAGE was run in tris-glycine running buffer at 130 V and stained with InVision™ His Tag stain (Thermo Fisher) followed by Coomassie stain. Using the QTRP 5600 Triple-Quad time of flight mass spectrometer (AB SCIEX), we confirmed the molecular weight of each protein indicating successful expression of the plasmid of interest (**Figure S1**, **S2**, **S3**, **S4**, **S5**, **S6**).

2.4 HYDROGEL PREPARATION

Following protein expression and purification, lyophilized protein was resuspended in phosphate-buffered saline (PBS, pH 7.4) at 10% (w/w). Gels were vortexed, centrifuged, incubated at 37 °C for 10 min, and gently rocked at 4 °C overnight to encourage uniform gel formation. For cell encapsulation studies, lyophilized protein was rehydrated in cell suspension at 10% (w/w) and incubated for 1 hour at 37 °C (or until gels were uniform) and gently mixed by a pipette tip.

2.5 RHEOLOGY

Characterization of material properties was performed using a Physica MCR 301 Rheometer with a parallel plate geometry (8 mm plate diameter, 500 μm gap) and a Peltier plate for temperature control. Once the geometry reached the measurement position, mineral oil was applied to the surrounding edges of the gel to prevent evaporation. The rheology protocol was adapted from the Burdick group[45]. The first segment included a 200 s oscillatory time sweep at constant strain (5%) and frequency (30 rad s^{-1}) to ensure proper mixing and plateau storage modulus. Next, an angular frequency sweep was performed at constant strain (5%) with varied frequency (0.1 – 100 rad s^{-1}) to identify the linear viscoelastic range (LVER) followed by another time sweep to reset the gel. Then a strain sweep was implemented at constant frequency (30 rad s^{-1}) with varied strain (0 – 500%) to identify LVER followed by another time sweep to reset the gel. Subsequently, the cyclic strain sweep test was employed by toggling between low (5% strain, 30 min, within LVER) and high (500% strain, 1 min, outside of LVER) strain 4 times at constant angular frequency (30 rad s^{-1}, within LVER). Finally, a rotational shear thinning test at increasing shear rate (0.1 – 50 s^{-1}) was implemented to demonstrate decreasing viscosity with increasing shear. A total of five replicates were repeated for each gel type (PXP, T40A, Q54A, and T40A + Q54A). All tests were performed at 25 °C (relevant for injection temperature) followed by 37 °C (body temperature).

Analysis of rheology data was automated in Python[46] to calculate the average storage modulus, strain crossover, frequency crossover, and recovery time for each gel and condition. The storage modulus was calculated as the average of the last 25 data points in the first and second time sweeps. Strain and frequency crossovers were interpolated to determine when G” (loss modulus) > G’ (storage modulus) during the corresponding strain and frequency sweep tests.

Recovery time crossover was interpolated as the time it takes to recover back to the gel state (G' > G") after periods of high strain during the cyclic strain sweep test. A multiple comparisons two-way ANOVA table was applied for statistical analysis to determine significance between mutant types.

2.6 BIODEGRADATION

For biodegradation studies, 50 μL gels (N=3 per gel type) at 10% (w/w) were formed in the bottom of a 15 mL Falcon™ tube and washed twice with 5 mL PBS + 0.75 mM phenylmethylsulfonyl fluoride (PMSF) to remove any initially unincorporated protein. 10 mL of fresh PBS containing 0.75 mM PMSF was replaced on top of the gel and the tubes were incubated at 37 °C for the remainder of the study. Time points were taken every 24 hrs by centrifugation of samples at 200 x g for 1 minute followed by removal of 100 μL fluid for later analysis. To replace the fluid removed, 100 μL fresh PBS containing 0.75 mM PMSF was added back to each sample. The test continued for 32 days at which point intact gel was still visible at the bottom of the tube.

Protein concentration in the supernatant at each time point was used to determine extent of gel erosion. A bicinchoninic acid (BCA) assay with a standard curve of known PXP concentrations ranging from 5 – 700 μg mL^{-1} was utilized to quantify protein concentration in the samples. Samples were measured in technical duplicates on a 96-well plate, and fluorescence was detected ($\lambda_{emission}$ = 562 nm) on a plate reader. Values were adjusted based on the total protein mass in each wash sample, the amount of protein removed at each time point, and evaporation in the tubes throughout the course of the study to obtain the final values for analysis.

2.7 iPSC-CM INJECTION PROTECTION

Human iPSC-CMs derived from RUES2 stem cells[5] were gifted by Mary O'Kelly Boit (Murry and DeForest Labs, University of Washington) and resuspended at a concentration of 10 million cells within 100 μL of 10% (w/w) PXP gels and pro-survival cocktail (PSC) components (Pro-survival cocktail: RPMI-based pro-survival cocktail for cell implantation containing 50% (vol/vol) growth factor-reduced Matrigel™, 100 μM ZVAD (benzyloxycarbonyl-Val-Ala- Asp(O-methyl)-fluoromethyl ketone), 50 nM Bcl-XL BH4 (cell-permeant TAT peptide), 200 nM cyclosporine A, 100 ng mL^{-1} IGF-1, and 50 μM pinacidil.). The injectate was pushed through a 26 G needle at 20 μL s^{-1}. As a control, another suspension of 10 million cells within a liquid-only PSC was also injected for comparison. Cell viability was analyzed directly after injection using an NC200™ NucleoCounter®. Final cell populations included technical duplicate with N=15 per sample group. A multiple comparisons one-way ANOVA table was implemented for statistical analysis. These studies consisted of male iPSC-CMs; future studies will utilize and compare findings with female-derived cell lines.

2.8 72 HOUR ENCAPSULATION OF FIBROBLASTS AND iPSC-CMS

NIH 3T3 Fibroblasts gifted from the Dr. Jennifer Davis lab (University of Washington) were suspended as 5 million cells per mL in media (DMEM supplemented with 10% Fetal Bovine Serum and 1% Penicillin/Streptomycin). Human iPSC-CMs were suspended as 10 million cells per mL in media (RPMI supplemented with 2% B-27 and 10% Penicillin/Streptomycin).

Cell suspensions (Fibroblast or iPSC-CM) were added directly to lyophilized PXP protein resulting in 10% (w/w) gels. Encapsulated cells, and a cell-only control group, were injected in triplicate at a volume of 20 μL per well (384-well plate) through a 26 G needle. Two additional

groups were added for the iPSC-CM study, including a cell suspension in PSC (as described in injection protection methods) and cells encapsulated in PXP at 10% (w/w) with PSC. 20 μL of fresh media was added to each well, then the plate was incubated for 24 hrs at 37 °C.

Cells were stained with 4 μM CalceinAM ($\lambda_{excitation}$ = 488 nm, $\lambda_{emission}$ = 520 nm) and 8 μM Ethidium Homodimer-1 ($\lambda_{excitation}$ = 580 nm, $\lambda_{emission}$ = 604 nm) then imaged on a Leica Stellaris 5 Confocal through the full thickness of each sample with a step size of 3 μm in the z direction. Viability was quantified using the Leica Application Suite X (LAS X) software by implementation of an Otsu threshold for both channels (CalceinAM and Ethidium Homodimer-1). Cells were incubated at 37 °C for an additional 48 hrs, and final cell viability of each well was analyzed using an NC200™ NucleoCounter®. A multiple comparisons one-way ANOVA table was implemented for statistical analysis.

2.9 PROTEIN OF INTEREST FUNCTIONALIZATION

To model the incorporation of a protein of interest, PeGFP (eGFP with a single P domain) was added to the PXP gels. Lyophilized PXP was rehydrated with either PeGFP or eGFP (without a P domain) in phosphate buffer both resulting in an eGFP molar concentration of 84 μM throughout the gel (6.5% of the pentameric P domain interactions functionalized with a PeGFP). 50 μL gels (N=3) were formed in the bottom of 1.5 mL Eppendorf™ tubes at 10% (w/w) PXP and 500 μL phosphate buffer was added to the top of each. 2 μL fluid was removed every hour, diluted in 23 μL phosphate buffer, and fluorescence was monitored in a 384-well plate until a plateau concentration occurred ($\lambda_{excitation}$ = 488 nm, $\lambda_{emission}$ = 530 nm). Fluorescence standard curves of known PeGFP and eGFP concentrations ranging from 0.02 – 5 μM were employed to quantify

eGFP released. If functionalization is successful, the PeGFP should release at a slower rate than eGFP without a P domain.

Chapter 3. RESULTS

3.1 INJECTABILITY AND RECOVERY OF GELS

Purified PXP proteins yielded stable hydrogels when reconstituted with PBS at 10% (w/w) and were macroscopically injectable through a 26 G needle at room temperature (25 °C) and physiologically relevant temperature (37 °C) (**Figure 1d, e**). We expected to see shear-thinning and self-healing behavior in rheological assessment. Additionally, we expected the introduction of point mutations (T40A, Q54A, or both T40A + Q54A) to stabilize coiled-coil interactions by exchanging two polar residues to a smaller hydrophobic alanine and allow for improved association between P domains[28,44].

Strain sweeps identified a strain crossover for each gel type indicating the injectable nature of PXP and mutants by moving from an elastic material at low strain (G' > G") to a viscous material at high strain (G' < G") (**Figure 2a**). The strain crossover at 37 °C confirmed breaking of physical coiled-coil bonds under high strain and occurs at 151 ± 5% strain for PXP, 143 ± 7% strain for T40A, 132 ± 13% strain for Q54A, and 95 ± 12% strain for T40A + Q54A, allowing for successful injection through a 26 G needle (**Table 1**). Interestingly, we observed a statistically significant decrease ($p < 0.01$) in strain crossover with the introduction of both P domain mutations (T40A + Q54A), which does not align with what we expected to see for stabilizing coiled-coil interactions (**Figure 2c)**. However, we expect the strain crossover is sufficiently high for all PXP mutants to avoid strain-induced liquification through beating-associated heart contraction.

The frequency sweeps indicate that with increasing frequencies, elastic properties are favored over viscous properties (G' > G") as there is minimal time for hydrogels to flow at higher frequencies. Frequency sweeps identified the angular frequency crossover to define the elastically

favored region (in the gel state), which was extended with mutated P domains (**Figure 2b**). No frequency crossover was found for Q54A or T40A + Q54A, indicating a larger working range of frequencies for these materials. In addition, the T40A crossover at 2.5 ± 0.4 rad s^{-1} was lower than the unmodified PXP at 12.0 ± 1.8 rad s^{-1}, which extended the frequency LVER (37 °C) (**Figure 2d, Table 1**). The human heart beats between 6.3 – 10.5 rad s^{-1}, meaning the best material selection would include the heart frequencies within the LVER, such as with Q54A or T40A + Q54A.[47]

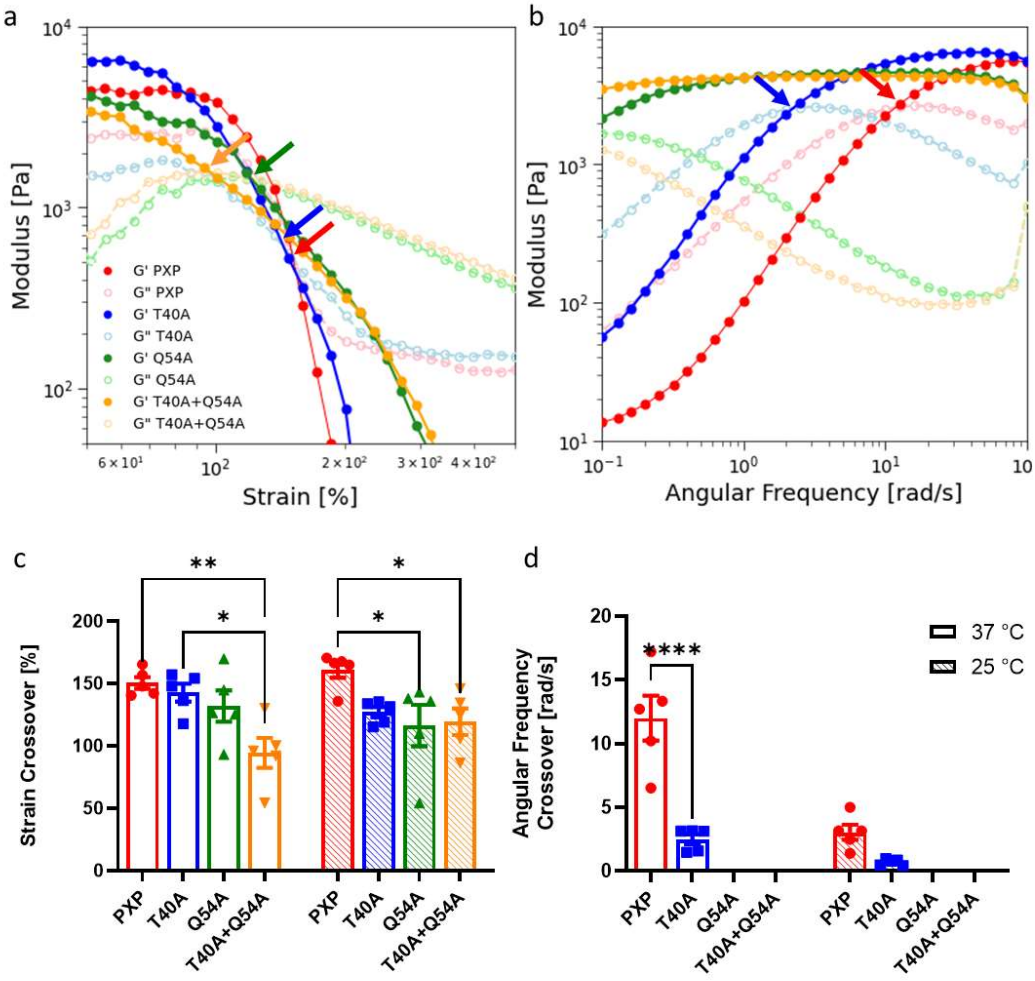

Figure 2. Rheometric analysis of coiled-coil protein-based hydrogels. G': storage modulus represented by dark-colored closed circles, G": loss modulus represented by light-colored open circles. PXP in red, T40A in blue, Q54A in green, and T40A + Q54A in orange. a) Strain sweeps for all gel types at 37 °C and 30 rad s^{-1} from 0 – 500% strain. Shear-thinning or

injectable behavior is observed for all gel types by strain crossover points (G" > G') indicated by colored arrows. b) Frequency sweeps for all gel types at 37 °C and 5% strain from 0.1 – 100 rad s^{-1}. Frequency crossover points indicated by colored arrows. A lengthened linear viscoelastic range (LVER) is observed after the introduction of point mutations as demonstrated by the length of plateau storage modulus (G') in frequency sweeps. c) Strain crossover values reported from strain sweeps showing a statistically significant decrease ($p < 0.05$) in strain crossover with the introduction of both mutations (T40A + Q54A) at 37 °C and 25 °C. c) Frequency crossover reported from frequency sweeps indicating improved stability with mutations due to increased LVER (no crossover for Q54A and T40A + Q54A). A multiple comparisons two-way ANOVA table was implemented for mutant comparison (* $p < 0.05$, ** $p < 0.01$, **** $p < 0.0001$).

The storage modulus (G') of PXP and mutants fall between 3.8 – 6.1 kPa (PXP, 4.5 ± 0.5 kPa; T40A, 6.6 ± 1.3 kPa; Q54A, 4.0 ± 0.9 kPa; T40A + Q54A, 4.5 ± 0.4 kPa) during time sweeps at constant 5% strain and 30 rad s^{-1} frequency, which is within range for materials that have been reported in the past for injectable heart cell therapies (approximately 0.5 – 5 kPa)[15–17]. No statistical significance was found between the storage moduli of mutants (**Figure 3d, Table 1**).

Cyclic strain sweeps were employed to test the self-healing behavior and recovery time of each gel type. The operating frequency for cyclic strain sweep tests was within the LVER for all mutants at both temperatures (30 rad s^{-1}). The high strain value was well above the crossover strain for all mutants (500%), and the low strain was below crossover strain for all mutants (5%). Cyclic strain sweeps confirmed self-healing behavior for all gels, or the reforming of coiled-coil physical bonds upon return to low strain. We observed full gel recovery and minimal hysteresis (**Figure 3a**) after 4 cycles of high strain for all gel types and a recovery time of 7.91 ± 2.23 s for PXP, 4.58 ± 0.12 s for T40A, 4.39 ± 0.04 s for Q54A, and 4.38 ± 0.05 s for T40A + Q54A at 37 °C (**Figure 3b, c**, **Table 1**). We found a statistically significant ($p < 0.05$) 3 s reduction in recovery time by

the introduction of point mutations due to highly favorable interactions of the stabilized mutated P domains.

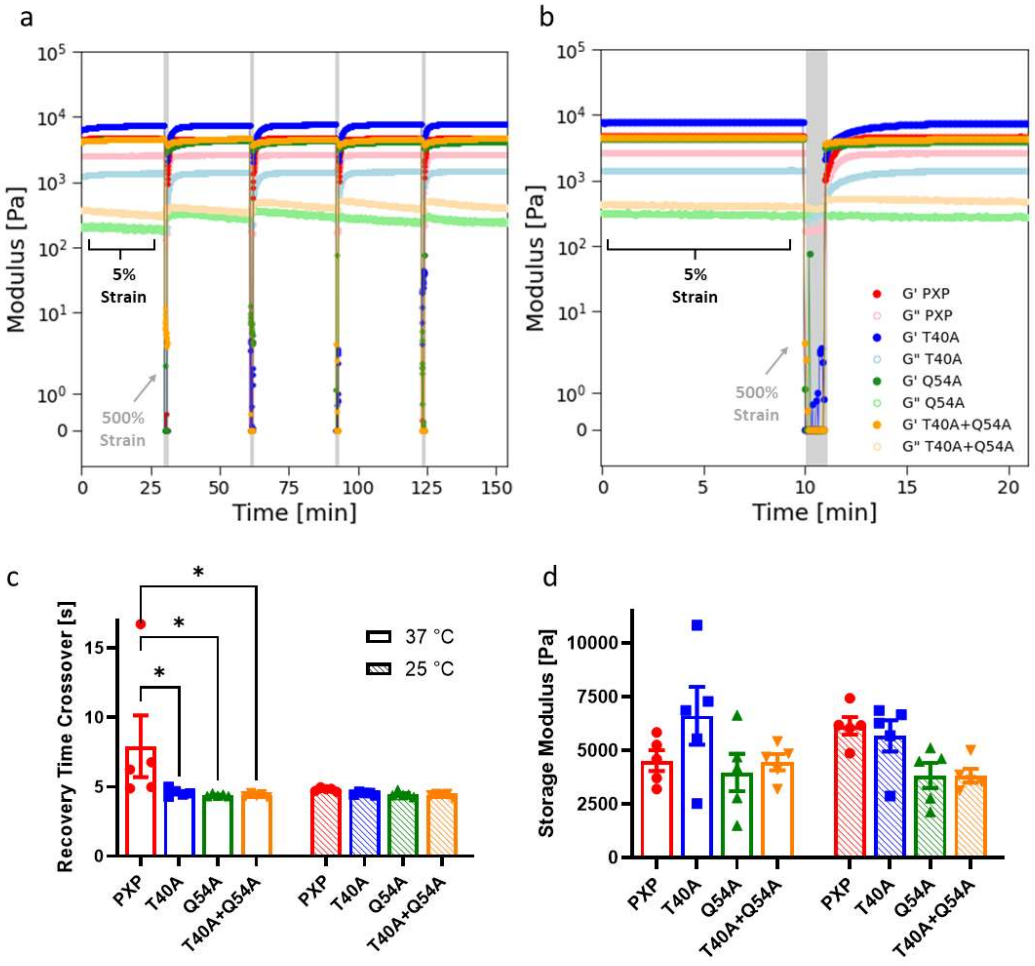

Figure 3. Self-healing properties of coiled-coil protein-based hydrogels. G': storage modulus represented by dark-colored closed circles, G": loss modulus represented by light-colored open circles. PXP in red, T40A in blue, Q54A in green, and T40A + Q54A in orange. a) Cyclic strain sweep test at 37 °C and 30 rad s^{-1} with 5% low strain value and 500% high strain value (highlighted in gray). Full recovery is achieved for each gel type after each of 4 periods of high strain. b) Zoom of a representative high strain period from the cyclic strain sweep. Visually slower recovery of PXP is observed when compared to the mutants. c) Average recovery time crossover, when G' > G" after the high strain period, is improved for mutants by 3 s at 37 °C. d) Average storage modulus for each gel type (10% w/w) and temperature conditions with no

statistical difference between mutants. A multiple comparisons two-way ANOVA table was implemented for mutant comparison (* $p < 0.05$).

Table 1. Summary of rheological properties for each gel at 25 °C and 37 °C. Storage modulus calculated from time sweeps (5% strain, 30 rad s^{-1}). Strain crossover (G" > G') calculated from strain sweeps (30 rad s^{-1}, 0 – 500% strain). Frequency crossover calculated from frequency sweeps (5% strain, 0.1 – 100 rad s^{-1}, G' > G"). No frequency crossover was observed for Q54A or T40A+Q54A. Recovery time crossover (G' > G" after high strain period) calculated from cyclic strain sweeps (30 rad s^{-1}, 5% low strain, 500% high strain). Error reported as SEM, N=5.

Parameter	**Temp [°C]**	**PXP**	**T40A**	**Q54A**	**T40A+ Q54A**
Storage Modulus [kPa]	25	6.1 ± 0.4	5.7 ± 0.7	3.8 ± 0.6	3.8 ± 0.3
	37	4.5 ± 0.5	6.6 ± 1.3	4.0 ± 0.9	4.5 ± 0.4
Strain Crossover [%]	25	161 ± 6	127 ± 4	116 ± 17	119 ± 11
	37	151 ± 5	143 ± 7	132 ± 13	95 ± 12
Frequency Crossover [rad s^{-1}]	25	3.0 ± 0.6	0.7 ± 0.1	-	-
	37	12.0 ± 1.8	2.5 ± 0.4	-	-
Recovery Time Crossover [s]	25	4.79 ± 0.06	4.51 ± 0.05	4.45 ± 0.09	4.39 ± 0.06
	37	7.91 ± 2.23	4.58 ± 0.12	4.39 ± 0.04	4.38 ± 0.05

3.2 TUNABLE BIODEGRADATION PROPERTIES

Biodegradation studies revealed gels incubated in PBS at 37 °C remain intact for up to 4 weeks, which is important for injectable cell therapies, as cells need support during early engraftment. We observed a slower degradation rate during the first 11 days for all mutants (T40A, Q54A, and T40A + Q54A) when compared to PXP, confirming the mutations stabilized physical association between P domains and allowing for tunable degradation profiles (**Figure 4**). The slowest erosion rate was observed in the double mutant (T40A + Q54A).

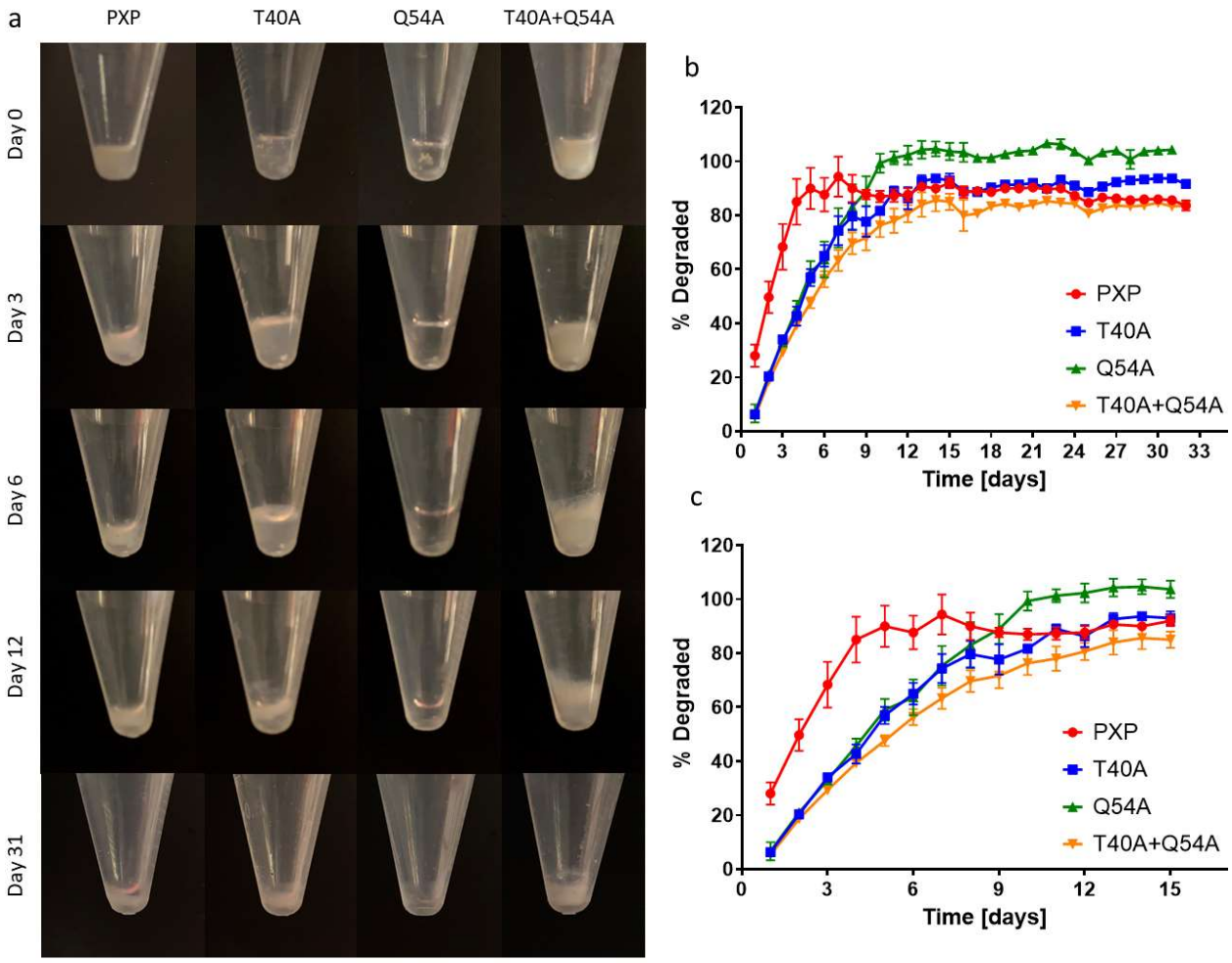

Figure 4. Biodegradation of 10% (w/w) PXP gels. a) Images at days 0, 3, 6, 12, and 31 of degradation in PBS at 37 °C for each gel type. Slowest degradation is observed in the T40A + Q54A mutant. Gels are visually intact after 31 days. b) BCA analysis of % degraded into PBS solution after incubation for 31 days. A plateau degradation is observed after the first 11 days for all gel types. c) % degraded during the first 15 days. Slower degradation is observed with the introduction of point mutations, with the slowest degradation being T40A + Q54A. Error bars reported as SEM, N=3.

3.3 iPSC-CM INJECTION PROTECTION

Encapsulating iPSC-CM in PXP prior to injection improved cell survival by more than 10%, allowing for additional cells to be delivered to the heart (pre-injection: 98.1% viability, post injection liquid suspension: 83.0% viability, post injection in 10% (w/w) PXP: 96.5% viability)

(**Figure 5**). This demonstrates cell protection during the injection process as hypothesized by alleviating shear stress on the cells thus reducing disruption to cell membranes and providing a scaffold environment post injection. Improved cell survival post injection is crucial to increasing the efficiency of these injectable cell therapies and chance of engraftment to the host tissue. Our results indicate PXP gels can be used as a delivery vehicle for injectable cardiomyocyte therapies.

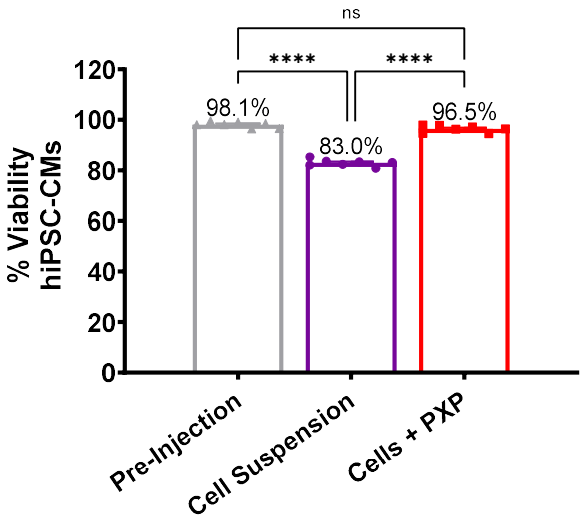

Figure 5. iPSC-CM injection protection. Viability of cells before injection (gray) and immediately after injection through a 26 G needle in cell suspension (purple) or encapsulated in PXP (red) determined by a NucleoCounter®. 10% improvement upon viability post injection by encapsulating cells within PXP. Statistically significant decrease in viability post injection of cell suspension. No significance between pre-injection and cells with PXP. A multiple comparisons one-way ANOVA table was implemented for statistical analysis (**** $p < 0.0001$, ns = not significant).

3.4 CELL VIABILITY THREE DAYS POST INJECTION

We observed an improved cell viability 24 hrs post-injection through a 26 G needle for NIH 3T3 fibroblasts encapsulated within PXP gels (88.6% viability) when compared to cell suspension alone (95.2% viability) visualized by CalceinAM and Ethidium Homodimer-1 staining

(**Figure 6a, b**). Additionally, a continued high viability is observed (by NucleoCounter®) 72 hrs post injection with no statistical difference between fibroblasts injected within PXP (93.4% viability) and cells that were not injected (97.6% viability). Alternatively, we do see a statistically significant decrease ($p < 0.001$) in viability of cells that were injected in liquid suspension (81.3% viability) (**Figure 6c**).

The iPSC-CMs also showed promising results 72 hrs post injection (**Figure 6d**). We observed no statistical significance between pre-injection control (89.1% viability) and cells encapsulated in PXP (93.7% viability). However, we do observe a statistically significant decrease ($p < 0.0001$) in viability with the cell suspension group (46.2% viability). We observed high viability for all groups injected with the PSC (**Figure 6e**). This indicates an added benefit that with the use of PXP, the PSC may no longer be necessary, which would reduce complications with FDA regulations and costs associated with PSC components. We are encouraged to see fibroblasts and iPSC-CMs have improved viability for up to three days post injection when compared to a cell suspension group demonstrating PXP cytocompatibility and offering 3D support to the cells.

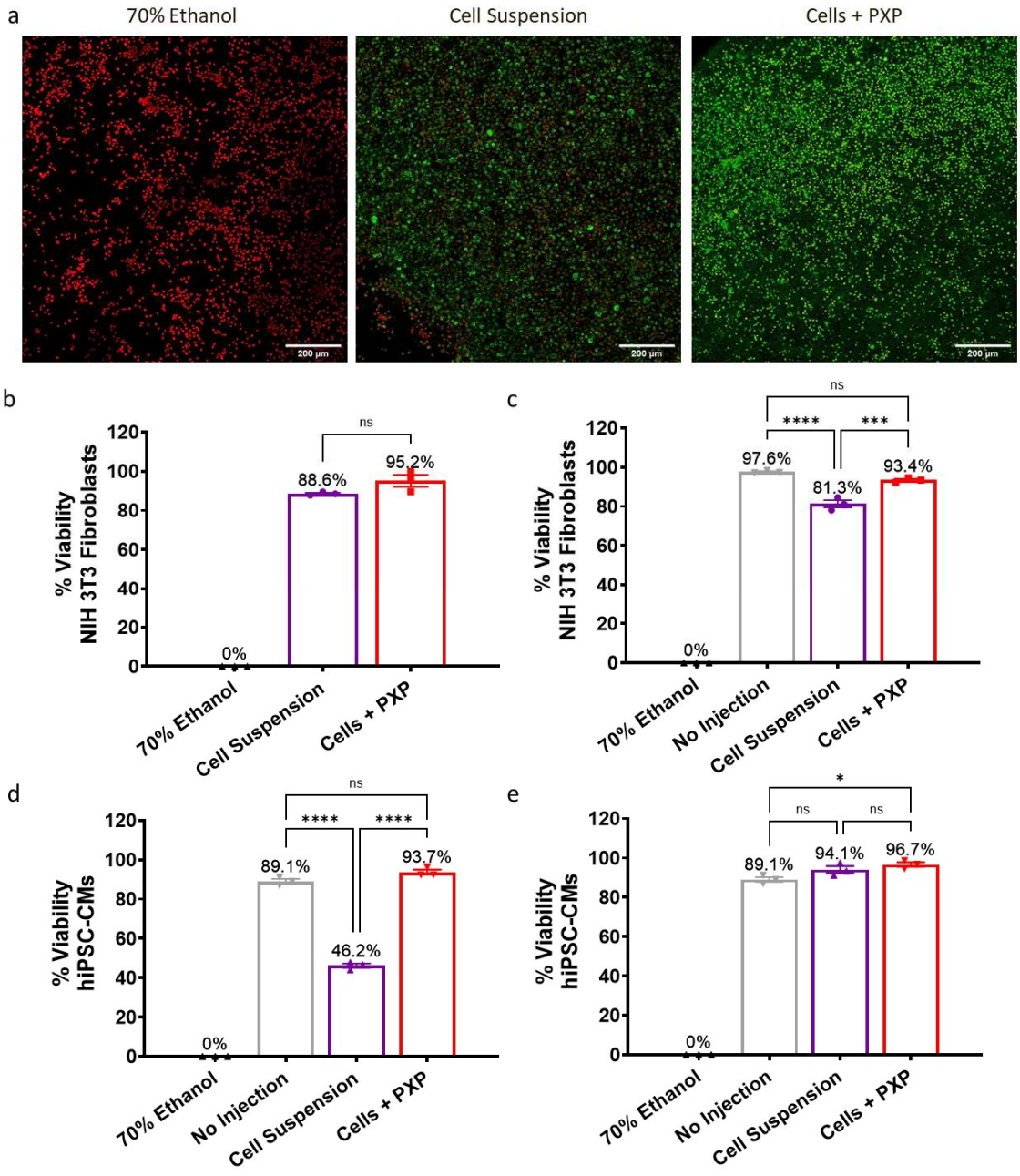

Figure 6. iPSC-CM and fibroblast viability 24 – 72 hours post injection. a) Confocal images of injected PXP encapsulated fibroblasts and injected fibroblast suspension group 24 hours post injection. CalceinAM stained for live cells (green) and Ethidium Homodimer-1 stained for dead cells (red). 70% ethanol treated cells were used as a dead control group. b) Fibroblast viability 24 hrs post injection quantified by live/dead count from confocal images in LAS X software. c) Fibroblast viability 72 hrs post injection quantified by a NucleoCounter®. d) iPSC-CM viability 72 hrs post injection quantified by a NucleoCounter®. e) iPSC-CM viability

with a pro survival cocktail (PSC) quantified by NucleoCounter®. One-way ANOVA tables were implemented for statistical analysis (* $p < 0.05$, *** $p < 0.001$, **** $p < 0.0001$, ns = not significant).

3.5 BIOFUNCTIONALIZATION

Therapeutic proteins including Delta-1 and erythropoietin have been integrated into gel networks to promote desired cell outcomes and facilitate healing process post myocardial infarction.[8,25] To demonstrate that biofunctionalization of PXP gels could be readily attained using proteins site-specifically modified with a single P domain, eGFP was selected as a model protein of interest due to its ability to be easily tracked by fluorescence. Attaching a single P domain to our model protein facilitates functionalization into the gel network. eGFP can be substituted for other user-defined therapeutic proteins.

PeGFP and eGFP were successfully expressed and purified as evidenced by SDS-PAGE and mass spectrometry (**Figure S6**). Fluorescence is observed in a 6.5% functionalized PXP gel, confirming that protein function is still in-tact with the addition of a single P domain (**Figure 7**c). Next steps will include comparing fluorescence release with eGFP to confirm functionalization.

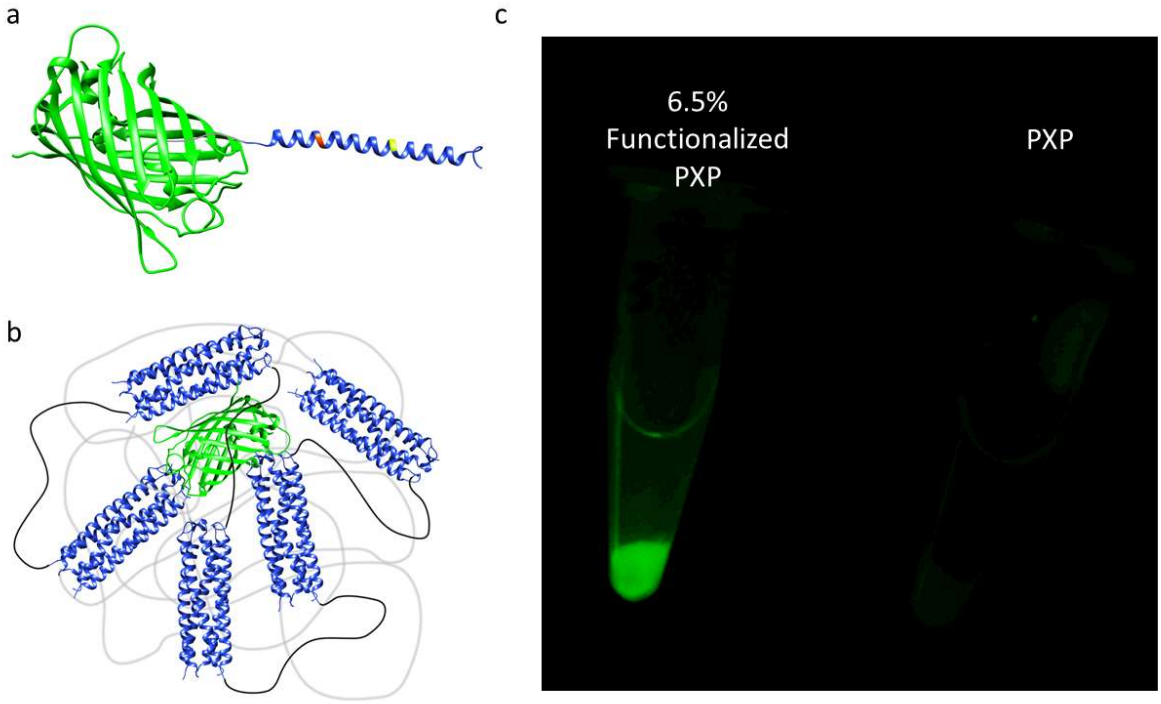

Figure 7. Bioconjugation of Protein of Interest. a) PeGFP contains a single P domain with both mutations (T40A in orange + Q54A in green) attached to eGFP. b) PXP gels are functionalized with the PeGFP protein. c) Fluorescence of PXP gel with 6.5% coiled-coil interactions functionalized with PeGFP (left) next to an unfunctionalized PXP gel (right) confirms proper refolding after denaturing purification ($\lambda_{excitation}$ = 488 nm, $\lambda_{emission}$ = 530 nm).

Chapter 4. CONCLUSION

Cell retention currently remains low for injectable iPSC-CM therapies in suspension (10% cell retention after three months[5]). Thus, there is an outstanding need for innovation of injectable biomaterials to improve the efficiency of therapeutic cell delivery to a damaged heart. Based on our findings, PXP gels are an excellent candidate for protecting cells during injection and early stages of engraftment. Our platform proposes a biocompatible synthetic protein, coil-XTEN-coil, which provides consistent manufacturing when compared to natural proteins and polymers that contain many species of varied length. The hydrogel is injectable, self-healing, and has the

potential to remain intact during early engraftment of cells, as shown by biodegradation studies for up to 4 weeks. Demonstrated by iPSC-CM encapsulation studies, PXP gels improved viability post injection by over 10% through a 26 G needle offering the cells protection from shear stress. Additionally, the cell viability remains high for up to 72 hours post injection. We are encouraged to observe improved cell survival post-injection indicating increased efficiency of cell therapies, such as iPSC-CM therapies for heart regeneration.

Our platform allows for user-tunable properties by introduction of point mutations in the P domains. We recommend use of the T40A + Q54A mutant, which has lengthened the viscoelastic range of working frequencies, decreased the gel recovery time by 3 seconds post injection, and slowed the degradation profile during the first 11 days. Furthermore, the user can add therapeutic proteins of interest to assist with cell engraftment. In summary, PXP gels provide biocompatibility, self-healing behavior, protection of cells during injection, and tunable properties for therapeutic cell delivery.

BIBLIOGRAPHY

1. WHO. Causes of Death. Published 2016. Accessed May 13, 2020. https://www.who.int/data/gho/data/themes/topics/causes-of-death/GHO/causes-of-death

2. Heron M. Deaths: Leading causes for 2017. *Natl Vital Stat Reports*. 2019;68(6).

3. Gerbin KA, Murry CE. The winding road to regenerating the human heart. *Cardiovasc Pathol*. 2015;24(3):133-140. doi:10.1016/j.carpath.2015.02.004

4. Hashimoto H, Olson EN, Bassel-Duby R. Therapeutic approaches for cardiac regeneration and repair. *Nat Rev Cardiol*. 2018;15(10):585-600. doi:10.1038/s41569-018-0036-6

5. Laflamme MA, Chen KY, Naumova A V., et al. Cardiomyocytes derived from human embryonic stem cells in pro-survival factors enhance function of infarcted rat hearts. *Nat Biotechnol*. 2007;25(9):1015-1024. doi:10.1038/nbt1327

6. Don CW, Murry CE. Improving survival and efficacy of pluripotent stem cell-derived cardiac grafts. *J Cell Mol Med*. 2013;17(11):1355-1362. doi:10.1111/jcmm.12147

7. Aguado BA, Mulyasasmita W, Su J, Lampe KJ, Heilshorn SC. Improving viability of stem cells during syringe needle flow through the design of hydrogel cell carriers. *Tissue Eng - Part A*. 2012;18(7-8):806-815. doi:10.1089/ten.tea.2011.0391

8. Gerbin KA, Mitzelfelt KA, Guan X, Martinson AM, Murry CE. Delta-1 functionalized hydrogel promotes hESC-cardiomyocyte graft proliferation and maintains heart function post-injury. *Mol Ther - Methods Clin Dev*. 2020;17(June):986-998. doi:10.1016/j.omtm.2020.04.011

9. Hao Y, Shoichet MS, Radisic M. Vascular endothelial growth factor immobilized in collagen scaffold promotes penetration and proliferation of endothelial cells. 2008;4:477-489. doi:10.1016/j.actbio.2007.12.011

10. Park JB, Bronzino JD. *CRC Handbook of Chemistry and Physics: A Ready-Reference Book of Chemical and Physical Data. Biologic Biomaterials: Tissue-Derived Biomaterials (Collagen)*.; 2000.

11. Amini AA, Nair LS, Lin G, Cosimbescu L. Injectable gels for tissue'75organ repair. Published online 2012:5-7. doi:10.1088/1748-6041/7/2/020201

12. Seif-naraghi SB, Horn D, Schup-magoffin PA, Christman KL. Injectable extracellular matrix derived hydrogel provides a platform for enhanced retention and delivery of a heparin- binding growth factor. 2013;8(10):3695-3703. doi:10.1016/j.actbio.2012.06.030.Injectable

13. Daly AC, Riley L, Segura T, Burdick JA. Hydrogel microparticles for biomedical applications. *Nat Rev Mater*. 2020;5(1):20-43. doi:10.1038/s41578-019-0148-6

14. Li Y, Xue B, Cao Y. Synthetic Protein Hydrogels. *ACS Macro Lett*. Published online 2020:512-524. doi:10.1021/acsmacrolett.0c00109

15. Rodell CB, MacArthur JW, Dorsey SM, et al. Shear-thinning supramolecular hydrogels with secondary autonomous covalent crosslinking to modulate viscoelastic properties in vivo. *Adv Funct Mater*. 2015;25(4):636-644. doi:10.1002/adfm.201403550

16. Sinclair A, O'Kelly MB, Bai T, Hung HC, Jain P, Jiang S. Self-Healing Zwitterionic Microgels as a Versatile Platform for Malleable Cell Constructs and Injectable Therapies. *Adv Mater*. 2018;30(39):1-8. doi:10.1002/adma.201803087

17. Sisso AM, Boit MO, Deforest CA. Self-healing injectable gelatin hydrogels for localized therapeutic cell delivery. 2020;(January):1112-1121. doi:10.1002/jbm.a.36886

18. Zheng A, Wu D, Fan M, et al. Injectable zwitterionic thermosensitive hydrogels with low-protein adsorption and combined effect of photothermal-chemotherapy. *J Mater Chem B*. 2020;8(46):10637-10649. doi:10.1039/d0tb01763a

19. Han Y, Yang J, Zhao W, et al. Biomimetic injectable hydrogel microspheres with enhanced lubrication and controllable drug release for the treatment of osteoarthritis. *Bioact Mater*. 2021;6(10):3596-3607. doi:10.1016/j.bioactmat.2021.03.022

20. Tu Y, Chen N, Li C, et al. Advances in injectable self-healing biomedical hydrogels. *Acta Biomater*. 2019;90(xxxx):1-20. doi:10.1016/j.actbio.2019.03.057

21. Wei Z, Zhao J, Chen YM, Zhang P, Zhang Q. Self-healing polysaccharide-based hydrogels as injectable carriers for neural stem cells. *Sci Rep*. 2016;6:1-12. doi:10.1038/srep37841

22. DeForest CA, Tirrell DA. A photoreversible protein-patterning approach for guiding stem cell fate in three-dimensional gels. *Nat Mater*. 2015;14(May). doi:10.1038/NMAT4219

23. Carlini AS, Gaetani R, Braden RL, Luo C, Christman KL, Gianneschi NC. Enzyme-responsive progelator cyclic peptides for minimally invasive delivery to the heart post-myocardial infarction. *Nat Commun*. 2019;10(1):1-14. doi:10.1038/s41467-019-09587-y

24. Traverse JH, Henry TD, Dib N, et al. First-in-Man Study of a Cardiac Extracellular Matrix Hydrogel in Early and Late Myocardial Infarction Patients. *JACC Basic to Transl Sci*. 2019;4(6):659-669. doi:10.1016/j.jacbts.2019.07.012

25. Chow A, Stuckey DJ, Kidher E, et al. Human Induced Pluripotent Stem Cell-Derived Cardiomyocyte Encapsulating Bioactive Hydrogels Improve Rat Heart Function Post Myocardial Infarction. *Stem Cell Reports*. 2017;9(5):1415-1422. doi:10.1016/j.stemcr.2017.09.003

26. Gaffey AC, Chen MH, Venkataraman CM, et al. Injectable shear-thinning hydrogels to deliver endothelial progenitor cells, enhance cell engraftment, and improve ischemic myocardium. *Physiol Behav*. 2016;176(1):139-148. doi:10.1016/j.physbeh.2017.03.040

27. Dooling LJ, Buck ME, Zhang W Bin, Tirrell DA. Programming Molecular Association and Viscoelastic Behavior in Protein Networks. *Adv Mater*. 2016;28(23):4651-4657. doi:10.1002/adma.201506216

28. Dooling LJ, Tirrell DA. Engineering the dynamic properties of protein networks through sequence variation. *ACS Cent Sci*. 2016;2(11):812-819. doi:10.1021/acscentsci.6b00205

29. Shen W, Zhang K, Kornfield JA, Tirrell DA. Tuning the erosion rate of artificial protein hydrogels through control of network topology. *Nat Mater*. 2006;5(2):153-158. doi:10.1038/nmat1573

30. Petka WA, Harden JL, McGrath KP, Wirtz D, Tirrell DA. Reversible hydrogels from self-assembling artificial proteins. *Science (80-)*. 1998;281(5375):389-392. doi:10.1126/science.281.5375.389

31. Rapp PB, Omar AK, Shen JJ, Buck ME, Wang ZG, Tirrell DA. Analysis and Control of Chain Mobility in Protein Hydrogels. *J Am Chem Soc*. 2017;139(10):3796-3804. doi:10.1021/jacs.6b13146

32. Malashkevich VN, Kammerer RA, Efimov VP, Schulthess T, Engel J. The crystal structure of a five-stranded coiled coil in COMP: a prototype ion channel? *Science (80-)*. 1996;274(5288):761-765.

33. Schellenberger V, Wang CW, Geething NC, et al. A recombinant polypeptide extends the in vivo half-life of peptides and proteins in a tunable manner. *Nat Biotechnol*. 2009;27(12):1186-1190. doi:10.1038/nbt.1588

34. Geething NC, To W, Spink BJ, et al. Gcg-XTEN: An improved glucagon capable of preventing hypoglycemia without increasing baseline blood glucose. *PLoS One*. 2010;5(4). doi:10.1371/journal.pone.0010175

35. Alters SE, McLaughlin B, Spink B, et al. GLP2-2G-XTEN: A Pharmaceutical Protein with Improved Serum Half-Life and Efficacy in a Rat Crohn's Disease Model. *PLoS One*. 2012;7(11). doi:10.1371/journal.pone.0050630

36. Bendele A, Seely J, Richey C, Sennello G, Shopp G. Short communication: Renal tubular vacuolation in animals treated with polyethylene-glycol-conjugated proteins. *Toxicol Sci*. 1998;42(2):152-157. doi:10.1006/toxs.1997.2396

37. Huang L, Gough PC, DeFelippis MR. Characterization of poly(ethylene glycol) and PEGylated products by LC/MS with postcolumn addition of amines. *Anal Chem*. 2009;81(2):567-577. doi:10.1021/ac801711u

38. Hong L, Wang Z, Wei X, Shi J, Li C. Antibodies against polyethylene glycol in human blood: A literature review. *J Pharmacol Toxicol Methods*. 2020;102(November 2019):106678. doi:10.1016/j.vascn.2020.106678

39. Podust VN, Balan S, Sim BC, et al. Extension of in vivo half-life of biologically active

molecules by XTEN protein polymers. *J Control Release*. 2016;240:52-66. doi:10.1016/j.jconrel.2015.10.038

40. Oldberg A, Antonsson P, Lindblom K, Heinegard D. COMP (cartilage oligomeric matrix protein) is structurally related to the thrombospondins. *J Biol Chem*. 1992;267(31):22346-22350. doi:10.1016/s0021-9258(18)41677-8

41. Hedbom E, Antonsson P, Hjerpe A, et al. Cartilage matrix proteins. An acidic oligomeric protein (COMP) detected only in cartilage. *J Biol Chem*. 1992;267(9):6132-6136. doi:10.1016/s0021-9258(18)42671-3

42. Sing MK, Burghardt WR, Olsen BD. Influence of End-Block Dynamics on Deformation Behavior of Thermoresponsive Elastin-like Polypeptide Hydrogels. *Macromolecules*. 2018;51(8):2951-2960. doi:10.1021/acs.macromol.8b00002

43. Guo Y, Bozic D, Malashkevich VN, Kammerer RA, Schulthess T, Engel J. All-trans retinol, vitamin D and other hydrophobic compounds bind in the axial pore of the five-stranded coiled-coil domain of cartilage oligomeric matrix protein. *EMBO J*. 1998;17(18):5265-5272. doi:10.1093/emboj/17.18.5265

44. Gunasekar SK, Asnani M, Limbad C, et al. N-terminal aliphatic residues dictate the structure, stability, assembly, and small molecule binding of the coiled-coil region of cartilage oligomeric matrix protein. *Biochemistry*. 2009;48(36):8559-8567. doi:10.1021/bi900534r

45. Chen MH, Wang LL, Chung JJ, Kim Y, Atluri P, Burdick JA. Methods To Assess Shear-Thinning Hydrogels for Application As Injectable Biomaterials. Published online 2017. doi:10.1021/acsbiomaterials.7b00734

46. Bennett J. Rheology. GitHub repository. https://github.com/jennybennett/rheology

47. Edward R. Laskowski MD. What's a normal resting heart rate? https://www.mayoclinic.org/healthy-lifestyle/fitness/expert-answers/heart-rate/faq-20057979

APPENDIX A

Table S1. Protein amino acid sequences. XTEN is highlighted in orange, P domains are highlighted in blue, **mutations** are highlighted in green, and RGD cell adhesion sites are highlighted in red.

Protein	Sequence
PXP (-RGD)	MRGSHHHHHHGSVDGSGSGSGSGSGSGAPQMLRELQETNAALQDVR ELLRQQVKEITFLKNTVMESDASGSGSGSGSGSGSLDGSPAGSPTSTE EGTSESATPESGPGTSTEPSEGSAPGSPAGSPTSTEEGTSTEPSEGSAPG TSTEPSEGSAPGTSESATPESGPGSEPATSGSETPGSEPATSGSETPGSP AGSPTSTEEGTSESATPESGPGTSTEPSEGSAPLDGSGSGSGSGSGSGA PQMLRELQETNAALQDVRELLRQQVKEITFLKNTVMESDASGSGSGS GSGSGSLEHHHHHHKLN*
PXP	MRGSHHHHHHGSGRGDSVDGSGSGSGSGSGSGAPQMLRELQETNAA LQDVRELLRQQVKEITFLKNTVMESDASGSGSGSGSGSGSLDGSPAGS PTSTEEGTSESATPESGPGTSTEPSEGSAPGSPAGSPTSTEEGTSTEPSEG SAPGTSTEPSEGSAPGTSESATPESGPGSEPATSGSETPGSEPATSGSET PGSPAGSPTSTEEGTSESATPESGPGTSTEPSEGSAPLDGSGSGSGSGSG SGAPQMLRELQETNAALQDVRELLRQQVKEITFLKNTVMESDASGSG SGSGSGSGSLEGRGDSHHHHHHKLN*
T40A	MRGSHHHHHHGSGRGDSGSGSGSGSGSGSGAPQMLRELQEANAALQ DVRELLRQQVKEITFLKNTVMESDASGSGSGSGSGSVDGSPAGSPTST EEGTSESATPESGPGTSTEPSEGSAPGSPAGSPTSTEEGTSTEPSEGSAP GTSTEPSEGSAPGTSESATPESGPGSEPATSGSETPGSEPATSGSETPGS PAGSPTSTEEGTSESATPESGPGTSTEPSEGSAPLESGSGSGSGSGSGAP QMLRELQEANAALQDVRELLRQQVKEITFLKNTVMESDASGSGSGSG SGSGSGRGDSHHHHHHKLN*
Q54A	MRGSHHHHHHGSGRGDSGSGSGSGSGSGSGAPQMLRELQETNAALQ DVRELLRQAVKEITFLKNTVMESDASGSGSGSGSGSVDGSPAGSPTST EEGTSESATPESGPGTSTEPSEGSAPGSPAGSPTSTEEGTSTEPSEGSAP GTSTEPSEGSAPGTSESATPESGPGSEPATSGSETPGSEPATSGSETPGS

	PAGSPTSTEEGTSESATPESGPGTSTEPSEGSAPLESGSGSGSGSGSGAP QMLRELQETNAALQDVRELLRQAVKEITFLKNTVMESDASGSGSGSG SGSGSGRGDSHHHHHHKLN*
T40A + Q54A	MRGSHHHHHHGSGRGDSGSGSGSGSGSGSGAPQMLRELQEANAALQ DVRELLRQAVKEITFLKNTVMESDASGSGSGSGSGSVDGSPAGSPTST EEGTSESATPESGPGTSTEPSEGSAPGSPAGSPTSTEEGTSTEPSEGSAP GTSTEPSEGSAPGTSESATPESGPGSEPATSGSETPGSEPATSGSETPGS PAGSPTSTEEGTSESATPESGPGTSTEPSEGSAPLESGSGSGSGSGSGAP QMLRELQEANAALQDVRELLRQAVKEITFLKNTVMESDASGSGSGSG SGSGSGRGDSHHHHHHKLN*
PeGFP	MRGSHHHHHHGSGSGSGSGSGSGSGAPQMLRELQEANAALQDVREL LRQAVKEITFLKNTVMESDASGSGSGSGSGSVDMVSKGEELFTGVVPI LVELDGDVNGHKFSVSGEGEGDATYGKLTLKFICTTGKLPVPWPTLV TTLTYGVQCFSRYPDHMKQHDFFKSAMPEGYVQERTIFFKDDGNYK TRAEVKFEGDTLVNRIELKGIDFKEDGNILGHKLEYNYNSHNVYIMA DKQKNGIKVNFKIRHNIEDGSVQLADHYQQNTPIGDGPVLLPDNHYL STQSALSKDPNEKRDHMVLLEFVTAAGITLGMDELYKKL*
eGFP	MRGSHHHHHHGSGSGSGSGSGSVDMVSKGEELFTGVVPILVELDGD VNGHKFSVSGEGEGDATYGKLTLKFICTTGKLPVPWPTLVTTLTYGV QCFSRYPDHMKQHDFFKSAMPEGYVQERTIFFKDDGNYKTRAEVKF EGDTLVNRIELKGIDFKEDGNILGHKLEYNYNSHNVYIMADKQKNGI KVNFKIRHNIEDGSVQLADHYQQNTPIGDGPVLLPDNHYLSTQSALSK DPNEKRDHMVLLEFVTAAGITLGMDELYKKL*

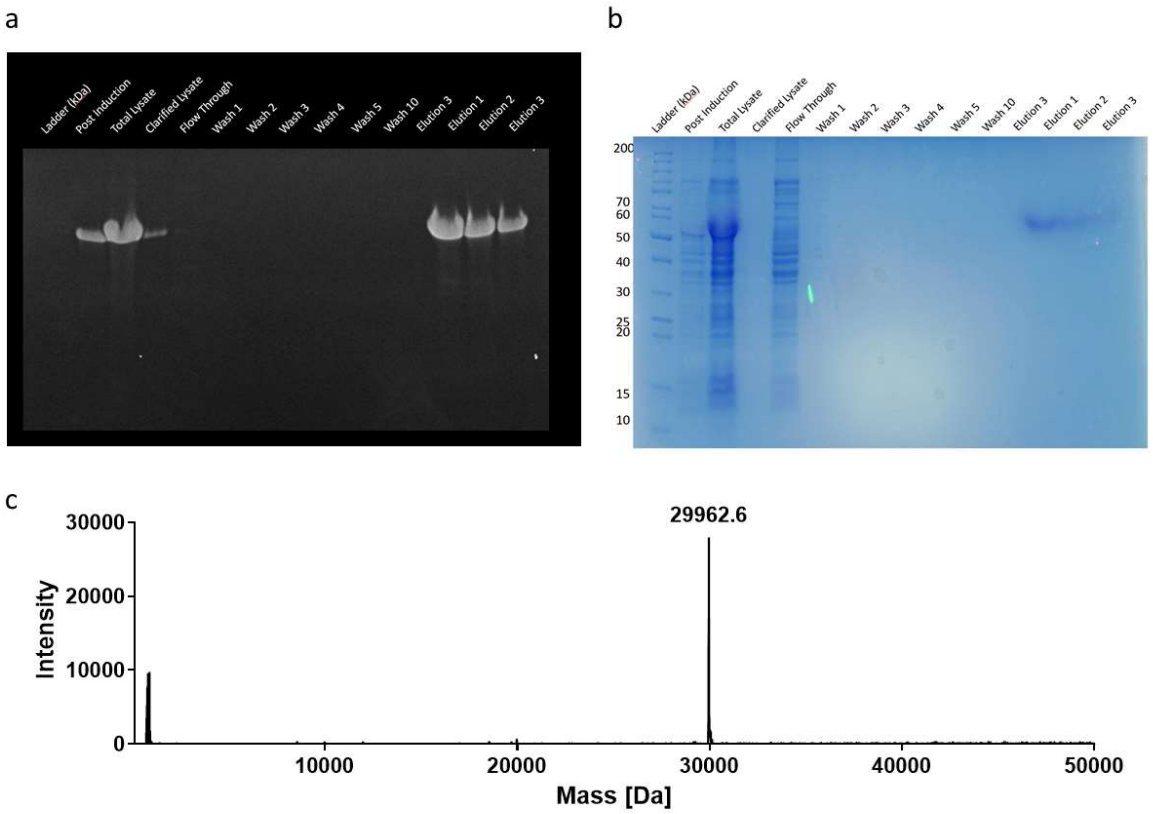

Figure S1. PXP (-RGD) verification. SDS-PAGE resulted in a pure product after Ni-NTA purification, as evidenced by a single band in the elution lanes corresponding to an apparent molecular weight of 60 kDa. The final product ran high due to weak binding to SDS caused by a lack of hydrophobic amino acids in XTEN[39]. a) Invision His tag stained SDS-PAGE. b) Coomassie stained SDS-PAGE. c) Mass spectrometry reported a final mass of 29,962.6 Da (calculated mass is 29,948.2 Da).

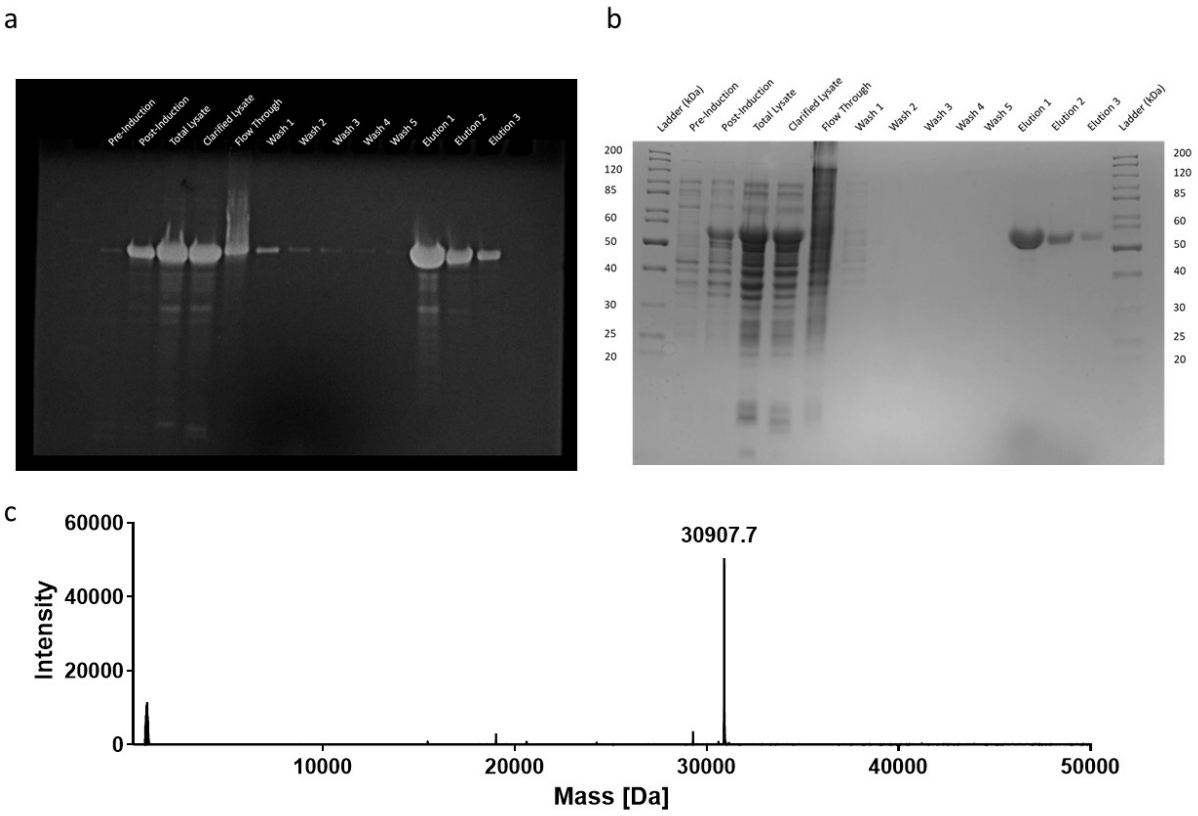

Figure S2. PXP (+RGD) verification. SDS-PAGE resulted in a pure product after Ni-NTA purification, as evidenced by a single band in the elution lanes corresponding to an apparent molecular weight of 60 kDa. The final product ran high due to weak binding to SDS caused by a lack of hydrophobic amino acids in XTEN[39]. a) Invision His tag stained SDS-PAGE. b) Coomassie stained SDS-PAGE. c) Mass spectrometry reported a final mass of 30,907.7 Da (calculated mass is 30,893.84 Da).

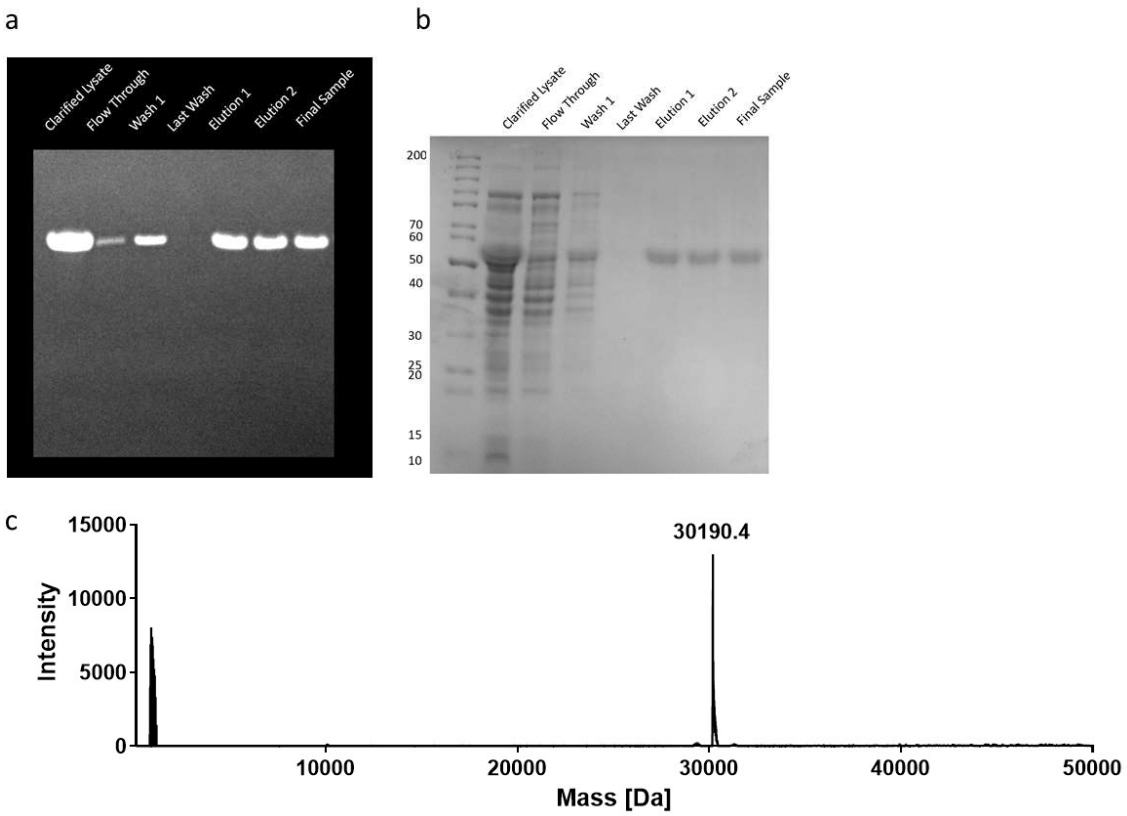

Figure S3. T40A verification. SDS-PAGE resulted in a pure product after Ni-NTA purification, as evidenced by a single band in the elution lanes corresponding to an apparent molecular weight of 60 kDa. The final product ran high due to weak binding to SDS caused by a lack of hydrophobic amino acids in XTEN[39]. a) Invision His tag stained SDS-PAGE. b) Coomassie stained SDS-PAGE. c) Mass spectrometry reported a final mass of 30,190.4 Da (calculated mass is 30,176.11 Da).

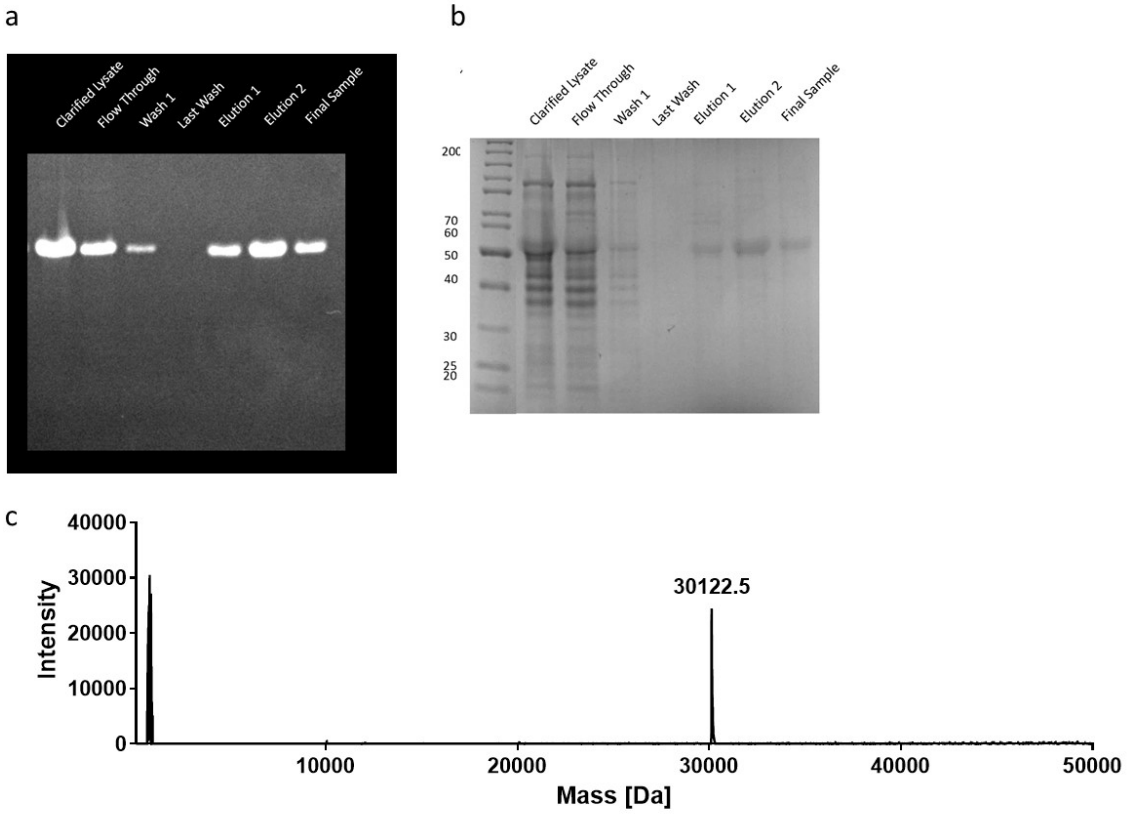

Figure S4. Q54A verification SDS-PAGE resulted in a pure product after Ni-NTA purification, as evidenced by a single band in the elution lanes corresponding to an apparent molecular weight of 60 kDa. The final product ran high due to weak binding to SDS caused by a lack of hydrophobic amino acids in XTEN[39]. a) Invision His tag stained SDS-PAGE. b) Coomassie stained SDS-PAGE. c) Mass spectrometry reported a final mass of 30,122.5 Da (calculated mass is 30,122.05 Da).

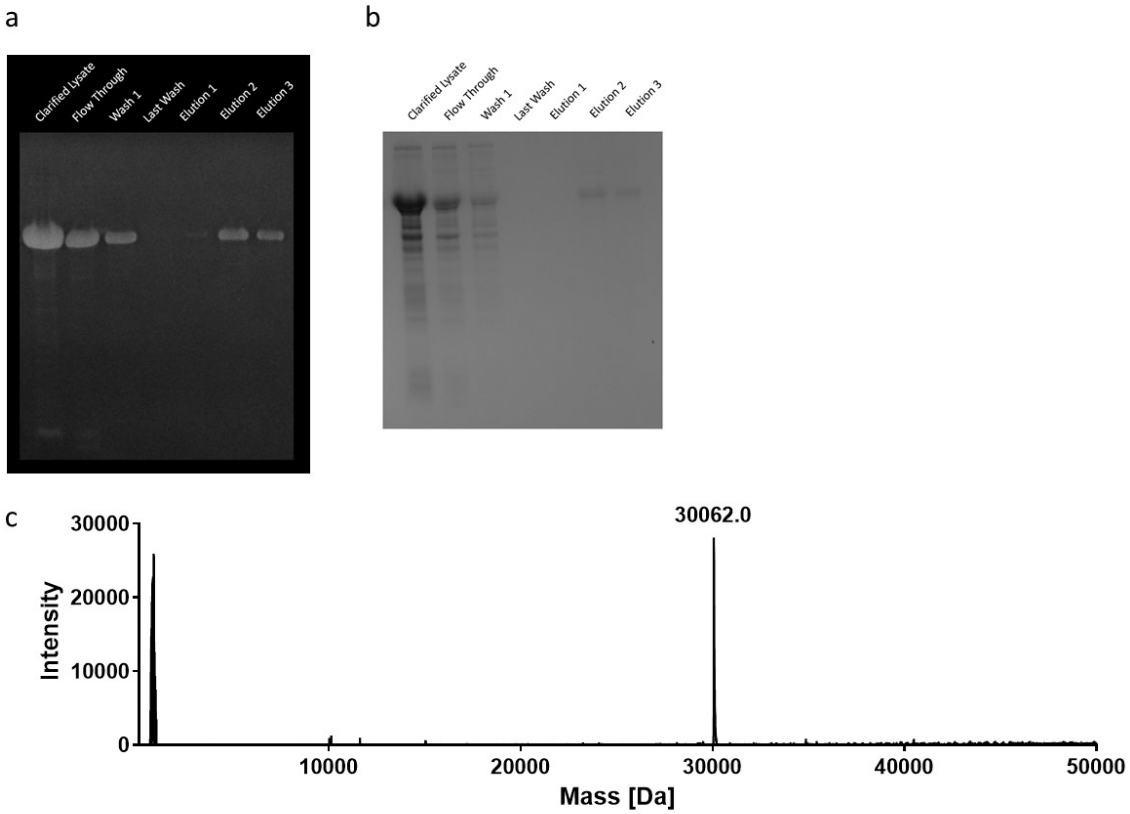

Figure S5. T40A+Q54A Verification. SDS-PAGE resulted in a pure product after Ni-NTA purification, as evidenced by a single band in the elution lanes corresponding to an apparent molecular weight of 60 kDa. The final product ran high due to weak binding to SDS caused by a lack of hydrophobic amino acids in XTEN[39]. a) Invision His tag stained SDS-PAGE. b) Coomassie stained SDS-PAGE. c) Mass spectrometry reported a final mass of 30,062.0 Da (calculated mass is 30,061.99 Da).

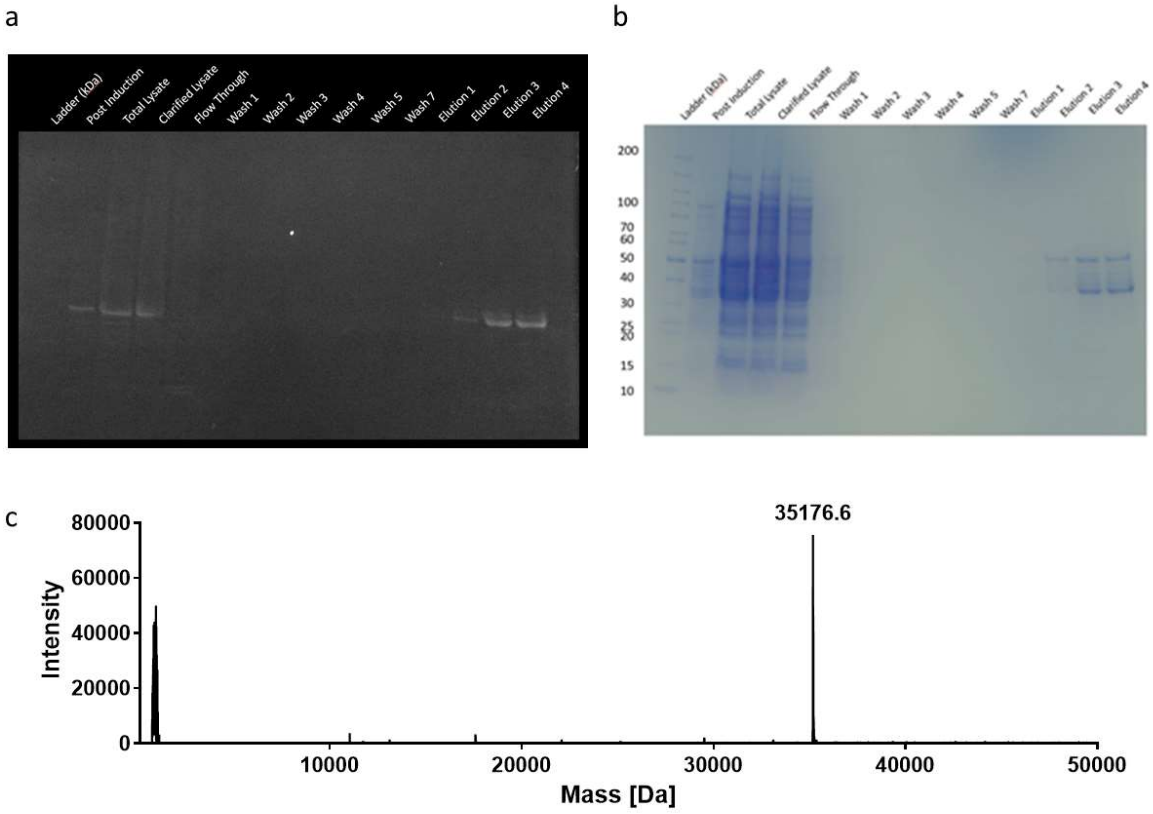

Figure S6. PeGFP Verification. a) SDS-PAGE gel with Invision His-tag stain shows successful single band of protein in lysate and elution samples. b) SDS-PAGE gel with Coomassie stain shows a dominant band corresponding to the product in the final elutions at 35 kDa. c) Mass spectrometry reported a final mass of 35,176.6 Da (calculated mass is 35,178.28 Da).

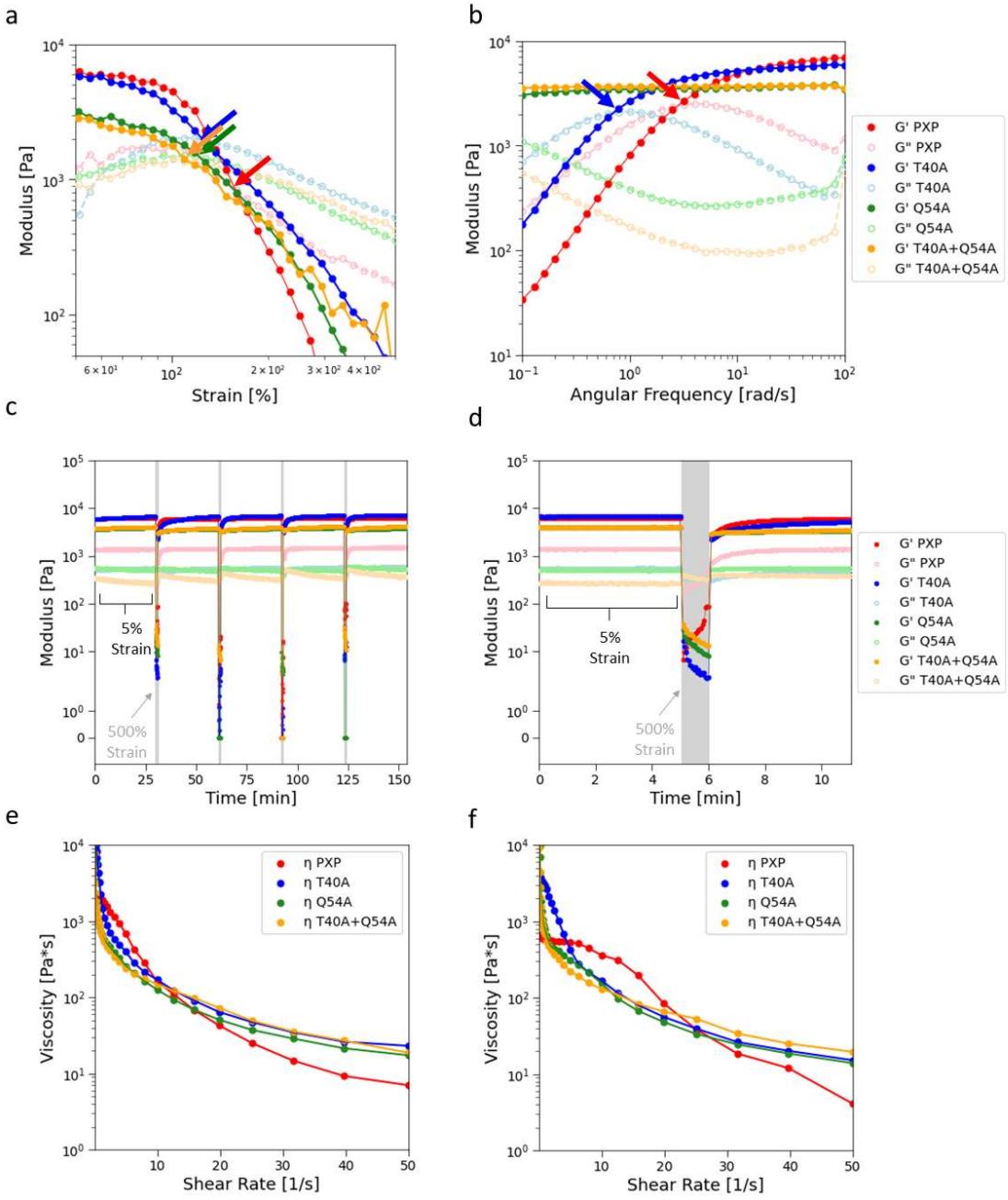

Figure S7. Strain and frequency sweeps at 25 °C and shear thinning tests at 25 °C and 37 °C. PXP in red, T40A in blue, Q54A in green, and T40A + Q54A in orange. a-d) G': storage modulus represented by dark-colored closed circles, G": loss modulus represented by light-colored open circles. a) Strain sweep at 25 °C (30 rad s^{-1}, 0 – 500% strain). b) Frequency sweep at 25 °C (5% strain, 0.1 – 100 rad s^{-1}). c) Cyclic strain sweep at 25 °C (30 rad s^{-1}, 5% low strain, 500% high strain in gray) demonstrating full recovery of all gels after 4 periods of high strain. d) Zoom on a representative high strain cycle of the cyclic strain sweep. e) Rotational shear

thinning test at room temperature (25 °C) indicating lowered viscosity at increased shear rates. f) Shear thinning test at physiological temperature (37 °C).